JOURNAL OF THERMOPHYSICS AND HEAT TRANSFER
Vol. 7, No. 3, July–Sept. 1993

Inverse Radiation Problem in Axisymmetric Cylindrical Scattering Media

M. P. Mengüç* and S. Manickavasagam†
University of Kentucky, Lexington, Kentucky 40506

A semianalytical technique has been developed to solve the inverse radiation problem in absorbing and scattering cylindrical media. The radiative properties in the medium are allowed to vary radially. Isotropic, linearly anisotropic, and Rayleigh scattering phase functions are considered, and both the first- and second-order scattering of radiation are accounted for in the analysis. The angular radiosity distribution obtained from the solution of the forward problem is employed as input to the inverse analysis. A numerical inversion scheme is followed to determine the profiles of extinction coefficient and the single-scattering albedo. For an anisotropically scattering medium, the asymmetry factor is also recovered. It is shown that the method is simple and accurate, even though the inversion is limited to three- or four-layer media. This inversion procedure can easily be used in experiments to determine the effective radiative property distributions in cylindrical systems.

Nomenclature

A = area
a,b = coefficients of the parabolic profiles
F = minimization quantity, Eq. (21)
g = asymmetry factor
I = intensity
L = distance traveled by the beam in the medium
l = beam-path in each layer
M = number of spatial locations used for incident laser
N = number of angular measurements for each spatial location
R = angular radiosity
s = line-of-sight path
V = volume
x,y = intersection points
α = scattering (zenith) angle
β = extinction coefficient
γ = scattering (zenigh) angle
θ = general scattering angle
κ = absorption coefficient
λ = wavelength
ρ = Levenberg-Marquardt parameter
σ = scattering coefficient
τ = optical thickness
Φ = scattering phase function
Ω = detector solid angle
ω = single-scattering albedo

Introduction

RADIATIVE transfer is the predominant mode of heat transfer in large-scale, particle-laden combustion systems, such as pulverized coal-fired furnaces. In order to design these systems effectively, radiative heat transfer must be modeled accurately. This requires 1) an accurate solution of the radiative transfer equation (RTE) in multidimensional, inhomogeneous media, and 2) accurate knowledge of the radiative properties of combustion gases and particles in the medium. The radiative properties of particles are more critical than that for gases for the accurate solution of the RTE, as the particles emit and absorb in the entire wavelength spectrum, whereas, the gases participate at only a few isolated narrow bands. The contribution of particles to radiative energy balance can be predicted if the intrinsic particle properties such as extinction, absorption, and scattering cross sections and scattering phase function are known. These properties are usually determined from theoretical models, such as the Lorenz-Mie theory, after making assumptions on the particle shape, size, size distribution, and complex index of refraction. Most of the time, these details are not available.

An alternative is to determine the required particle radiative properties directly from careful experiments. This can be accomplished by combining optical diagnostic techniques with an inverse radiation analysis. Here, an explicit (usually complicated) relation is found between the particle properties in the medium and the angular radiosity distribution measured by the detectors outside the medium. Such a relation is based on the solution of the radiative transfer equation for a given geometry. Then, the experiments are conducted and the medium properties are obtained using the measured quantities as input. This scheme works only if the inverse analysis is based on an algorithm which accurately relates the physics of the medium to the measured radiosities.

The inverse problem in nonscattering, cylindrical, axisymmetric systems has received considerable attention in the past. The formulation of this problem is based on the integral form of the radiative transfer equation as written along a line-of-sight. The solution can be obtained using an onion-peeling technique,[1] the Abel integral equation,[2,3] or a tomographic reconstruction technique.[2–9] If there are scattering particles, however, none of these techniques would be applicable. Solution of inverse radiation problem in planar, one-dimensional scattering media has been considered in a limited number of papers. McCormick[10–12] discussed many of these approaches in his review papers. A recent detailed literature search[13] has shown that medium inhomogeneities were accounted for in only a few studies.[13–15]

Inverse problems other than simple one-dimensional systems have not received much attention in the past. For multidimensional scattering systems, the only works published are those of Larsen.[16,17] The main reason for this is twofold; first, there is a lack of efficient direct solution methods for multidimensional, inhomogeneous, and anisotropically scattering media, which yield accurate radiative intensity distributions and can be employed in iterative or least-square minimization-based inversion schemes. Second, it is very difficult to develop inverse solution algorithms for general geometries which do not require the solution of the direct problem.

New approaches for the solution of inverse radiation problems in scattering, radially inhomogeneous cylindrical systems

Received Feb. 3, 1992; revision received July 20, 1992; accepted for publication July 27, 1992.

*Associate Professor, Department of Mechanical Engineering.
†Graduate Student, Department of Mechanical Engineering.

are very desirable, as these systems represent typical flame geometries. With this idea in mind, recently, an analytical tomographic reconstruction scheme has been developed for optically thin, single-scattering media[18] and its application to practical systems has been demonstrated.[9] Also, a statistical inverse Monte Carlo technique has been developed for multiple-scattering inhomogeneous media.[19] This article is to introduce a different approach, where a semianalytical inverse radiation analysis based on a direct formulation of the RTE with two successive orders of scattering is described. In all these studies, the physical system considered can be visualized as a laboratory flame. It is assumed that a narrow beam of laser is incident on the flame at different radial locations, and exit radiosities are measured at several angles.

It is worth noting that the inverse analysis presented here is to obtain the medium properties at a single wavelength; i.e., that of the incident light source. The radiant emission by the medium is not considered; it is assumed that the incident light is modulated using a beam chopper and the effects of all other radiation sources on the detector are filtered out. The properties recovered from the inverse analysis are local, spectral effective properties, i.e., for a given particle type and size distribution.

The structure of this article is as follows: first, the forward problem is formulated and the details of the formulation are discussed; a computational scheme is described to solve the inverse problem; numerical results obtained for the isotropic, Rayleigh, and linearly anisotropic scattering phase functions are reported, and the accuracy of the proposed scheme is evaluated.

Formulation of the Problem

Physical Model

Consider a narrow beam of collimated light (laser) incident on a cylindrical, radially nonhomogeneous, absorbing, and scattering medium. Assume several detectors are mounted on a circular platform around the medium and in the same plane as the laser beam. The solid angle subtended by each detector is considered to be very small, such that the variation of intensity within the solid angle can be assumed negligible. Such a small solid angle can be achieved by an appropriate combination of collection optics and apertures.

The energy of the laser beam is attenuated by the medium by means of absorption and scattering. Any detector receives a fraction of the scattered energy, if the direction of the scattered radiation coincides with the detector line-of-sight, $\overline{Q_1Q_2}$ (see Fig. 1). In order to calculate the amount of energy received by each detector, we have to consider all possible orders of scattering which eventually direct a fraction of scattered radiative energy towards the detector. Such a formulation, however, will be computationally very expensive. Instead, here we will consider only two orders of scattering.

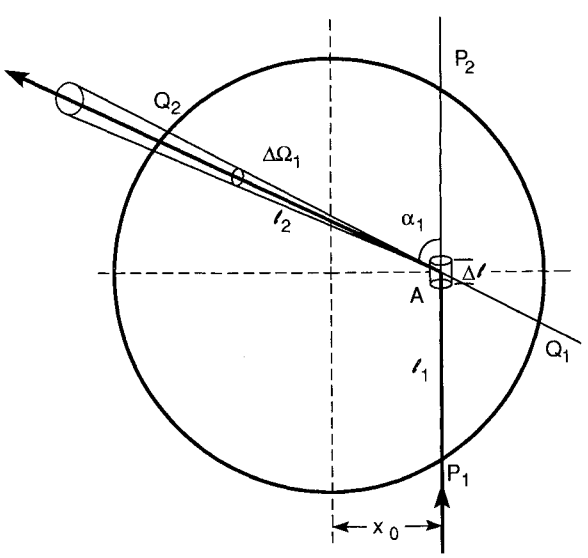

Fig. 1 Configuration and nomenclature for the first-order scattering.

It is well established that in homogeneous media, the single-order scattering assumption yields very accurate results if the medium optical thickness is less than 0.1. Recently, it was shown that for a polydispersed particle cloud, the single-scattering approximation is satisfactory if the optical thickness is less than 0.2, and two orders of scattering assumption yields very satisfactory agreement with the experimental data if the medium optical thickness is less than one.[21] The optical thickness of most laboratory flames, for which this model is developed, is less than one. Therefore, two orders of scattering assumption can be justified for our purposes.

One advantage of considering only two orders of scattering is that we don't have to account for azimuthal angle dependence of scattering angle. Since any photon scattered out of the plane defined by laser beam and detectors must be scattered two more times to be redirected towards the detector, we do not need to consider photons scattered out of the laser-detector plane anymore. This assumption is acceptable as long as the solid angle subtended by the detector is small.

The following derivation of the forward problem is based on a single discrete laser beam, incident on the medium at a distance x_0 from the axis of cylindrical section (see Fig. 1). Of course, the same formulation is valid for all $x_0 \in (0, R_0)$. If a laser sheet is used in the experiments, then a similar analysis is followed after dividing the beam into several discrete beams and then by summing the contributions from all of them.

Assume the energy of the laser beam at the boundary of the medium is $A_L I_0$, where I_0 is in units of $\mathrm{Wm^{-2}sr^{-1}}$, and A_L is the cross-sectional area of the cylindrical beam. Then, the intensity at any point along the path $\overline{P_1P_2}$ is given by

$$I(s) = I_0 \exp\left\{-\int_0^s \left[\kappa(s') + \sigma(s') - \sigma(s')\frac{\Phi(0, s')\Delta\Omega}{4\pi}\right] ds'\right\} \tag{1}$$

where κ and σ are the spatially and spectrally dependent absorption and scattering coefficients along the path s, $\Phi(0, s')$ is the scattering phase function in the forward direction, $\Delta\Omega$ is the small finite solid angle in the forward direction, and s' is the dummy spatial variable. For a homogeneous medium, Eq. (1) reduces to

$$I = I_0 e^{-\bar{\beta} l} \tag{2}$$

Here, $\bar{\beta}$ is the effective extinction coefficient of the medium and is given as

$$\bar{\beta} = \kappa + \sigma\{1 - [\Phi(0)\Delta\Omega/4\pi]\} \tag{3}$$

The correction factor due to the forward scattering (second term in the braces) is significant only if the phase function of the particles are highly forward scattering, such that $\Phi(0)\Delta\Omega/4\pi$ is not much smaller than unity. This is the case for large droplets or coal/char particles; otherwise, the correction term is not needed. (In theoretical calculations for intensity, $\Delta\Omega$ is infinitesimally small so that the correction term is not needed for any phase function. However, in experiments, $\Delta\Omega$ always has a finite value.)

Usually, practical systems such as flames are radially nonhomogeneous. We will model such a nonhomogeneous system as comprised of K concentric cylinders and assume properties are uniform and azimuthally symmetric in each of these cylindrical layers. Mathematically speaking, the accuracy of such an approximation increases with increasing K. Then, the optical path covered by the beam is given as

$$\bar{\beta} l = \sum_{i=1}^{K} \bar{\beta}_i l_i \tag{4}$$

where $\bar{\beta}_i$ is the extinction coefficient corresponding to layer i, l_i is the distance traveled by the particle within the layer, and l is the path covered by the beam in the medium.

First-Order Scattering

First, the formulation for the first-order scattering contribution of the laser beam on the detector reading is given. Consider that scattering takes place at small volume element V_A, which is at the intersection point of the laser beam and the detector line-of-sight. The intensity at A after attenuation along $\overline{P_1A}(=l_1)$ is written as

$$I_A = I_0 e^{-\bar{\beta} l_1} \tag{5}$$

where I_0 is the intensity of the incident laser beam and $\bar{\beta} l_1$ is given by Eq. (4). The radiation intensity (i.e., radiative energy per unit solid angle per unit area of the scattering volume) at the detector plane becomes

$$I_{D,1} = I_0 \frac{\sigma \Phi(\alpha_1)}{4\pi} \frac{dV}{dA} \exp[-\bar{\beta}(l_1 + l_2)] \tag{6}$$

The angular radiosity at the detector is given as

$$R_{D,1} = I_0[\sigma \Phi(\alpha_1)/4\pi] \exp[-\bar{\beta}(l_1 + l_2)] \Delta\Omega_1 A_L \Delta l \tag{7}$$

which is in units of watt. Here, α_1 is the scattering (zenith) angle, $\Delta\Omega_1$ is the solid angle subtended by the detector, $dV = A_L \Delta l$, Δl is the length of the laser beam along the scattering volume, and $A_L = 2\pi r_L$ is the cross-sectional area of the beam. A_L is assumed small enough that the properties of the medium can be considered uniform across the cross section of the laser beam. The distance l_2 is from A to the boundary of the medium ($l_2 = \overline{AQ_2}$).

Note that for nonhomogeneous media, $\bar{\beta} l_1$ and $\bar{\beta} l_2$ products are given by Eq. (4). Also note that in writing Eq. (7), we assumed an optical system is designed such that the scattering volume and the detector are at the object and image planes, respectively. The solid angle is small enough so that the scattering phase function does not vary within it. For larger solid angles, however, this variation must be accounted for.[21] In this analysis, A_L, $\Delta\Omega_1$, and Δl are constant.

Second-Order Scattering

To account for the second-order scattering contribution, we need to consider only the plane defined by the laser beam and the detector, as the detector solid angle is assumed very small. For this purpose, the first-order scattering from any point A along the original line-of-sight ($\overline{P_1P_2}$) of the beam should be accounted for (see Fig. 2). If the photons scattered at A reach a volume element B on $\overline{Q_1Q_2}$ and if they are rescattered towards the detector then their contribution is due to the second order scattering.

The intensity at any point B is written as

$$I_B = I_A[\sigma \Phi(\gamma_1)/4\pi] \, dl_1 e^{-\bar{\beta} l_2} \tag{8}$$

where I_A is given by Eq. (5). The intensity received by the detector is written as

$$I_D = I_B[\sigma \Phi(\gamma_2)/4\pi] \, dl_3 e^{-\bar{\beta} l_3} \tag{9}$$

The angular radiosity at the detector is then

$$R_{D,2} = I_0 A_L \int_0^{L_1} \int_0^{L_3} \sigma^2 \frac{\Phi(\gamma_1)}{4\pi} \frac{\Phi(\gamma_2)}{4\pi} \Delta\Omega_2 \cdot \exp[-\bar{\beta}(l_1 + l_2 + l_3)] \, dl_3 \, dl_1 \tag{10}$$

where, $L_1 = \overline{P_1P_2}$ and $L_3 = \overline{Q_1Q_2}$. Both scattering angles γ_1 and γ_3 are functions of l_1 and l_3. Note that, $\Delta\Omega_2$ is also a variable and a function of l_3; however, if the detectors are far away from the test region (i.e., focal length of the optical system used is large compared to the diameter of the flame), then we can safely assume that $\Delta\Omega_2$ is a constant and equal to $\Delta\Omega_1$ (see Fig. 1). The integrals in Eq. (10) can be evaluated using a Gaussian quadrature scheme (a 10-point scheme is used to obtain the results presented in this article).

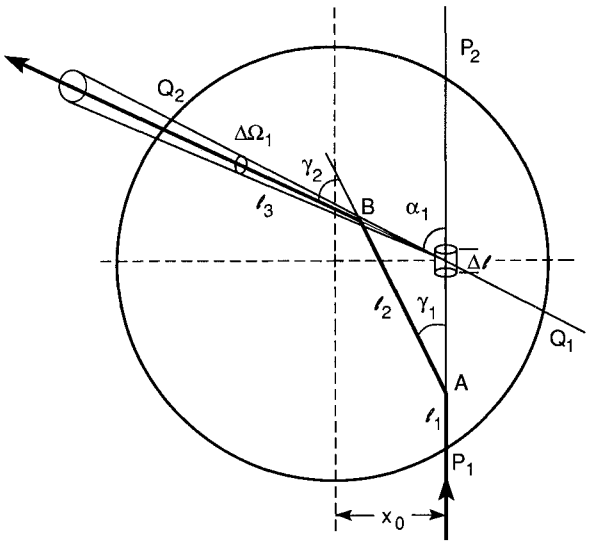

Fig. 2 Configuration and nomenclature for the second-order scattering.

The angular radiosity at the detector is determined by summing the contributions from the first- and second-order scattering

$$R_D(\theta) = R_{D,1}(\theta) + R_{D,2}(\theta) \tag{11}$$

This analysis should be slightly modified if a laser-sheet is used. First, the laser sheet is divided to several narrow beams, and for each of them the angular radiosity is determined from the above analysis, and then the total contribution is obtained. For the laser sheet application, it is preferable to focus the detector solid angle to the center of the test cell. For this case, the angular radiosity is written as

$$R(\theta) = \frac{\Delta w}{A_L} \int_{-Z_0}^{+Z_0} R_D(\theta) \, dz \tag{12}$$

where R_D is given by Eq. (11), and $2Z_0$ and Δw are the width and thickness of the beam, respectively. Here, the effect of laser beam cross section is explicitly written, therefore, the A_L terms used in Eqs. (7) and (10) appeared in the denominator of Eq. (12).

Calculation of Intermediate Paths in the Medium

Radially inhomogeneous medium is divided into several homogeneous concentric cylindrical layers, and the region between any two adjacent circles is called a layer. In each of these layers, the radiative properties, i.e., the absorption and scattering coefficients and the scattering phase function, are assumed to be constants. Equation (4) gives the attenuation along the path if the medium is nonhomogeneous. To calculate the path length of beam in each uniform layer, it is necessary to determine the points of intersection of the beam with the circles (layers) it crosses. Then, by choosing the appropriate points of intersection, the actual path length and the attenuation within the corresponding layer are calculated. In the present case, layers of equal thicknesses are considered; however, the methodology described below is applicable to any arbitrary division of layers. The procedure is as follows:

Let $A(x_1, y_1)$ be a point on $\overline{P_1P_2}$, and $B(x_2, y_2)$ on $\overline{Q_1Q_2}$. The equation for the line joining these two points is given as

$$y = mx + c \tag{13}$$

The equation for a circle is given as

$$x^2 + y^2 = a^2 \tag{14}$$

The points of intersection of the line with any circle of radius a are the roots of the quadratic formula, and determined as

$$x_{1,2} = \frac{-mc \pm \sqrt{D}}{(1 + m^2)} \tag{15}$$

$$y_{1,2} = mx_{1,2} + c \tag{16}$$

where

$$D = (1 - m^2)a^2 - c^2 \tag{17}$$

Then the path length in each circle is given by

$$l_i = \sqrt{(x_1 - x_2)^2 + (y_1 - y_2)^2} \tag{18}$$

where (x_1, y_1) and (x_2, y_2) are the points of intersection of the line with the adjacent circles. It is necessary to determine the points of intersection of the line with all the circles it crosses. Once the points intersecting the first layer is known, the distance between them is calculated and stored in an array. Similarly, the points intersecting other layers are determined and the distances are stored in the same array. This array is for the cumulative distances and the actual distance in each layer is obtained from simple algebraic manipulation.

It is important to consider all different orientation of paths followed by the beam in the medium to avoid any numerical singularity. There are total of six special cases to be considered

Case i

In Fig. 3a, we observe the line $\overline{AB}$ intersects only the circles whose radii are greater than $\overline{OP}$ and less than $\overline{OB}$. Circles with radii greater than $\overline{OP}$ but less than $\overline{OA}$ are intersected twice, and circles with radii greater than $\overline{OA}$ but less than $\overline{OB}$ are intersected once. Circles with radii greater than $\overline{OB}$ are not intersected. If a circle is intersected only once, it is necessary to eliminate one of the roots determined. In this case, only the roots near B are retained for calculations. A different version of this case is obtained if A and B points are reversed.

Case ii

In this case (Fig. 3b), the points A and B are in the same quadrant. Circles with radii greater than $\overline{OA}$ are intersected (only once). The roots found in other quadrants are eliminated.

Case iii

Unlike case ii, here (Fig. 3c) $\overline{AB}$ has a negative slope. Therefore, some circles can be intersected twice, although the line is in the same quadrant. If we examine carefully we can see that this case is similar to case i and the same procedure can be followed to obtain the required lengths.

Case iv

In this case (Fig. 3d), the line $\overline{AB}$ intersects the circles only once, and only one root is required for calculations.

Case v

This time (Fig. 3e), A and B lie on the x axis; therefore, the y coordinates are zero. After setting $y_{1,2} = 0$, the procedure outlined in case i can be followed. Note that A can be at $x = 0$ or at either side of the x axis.

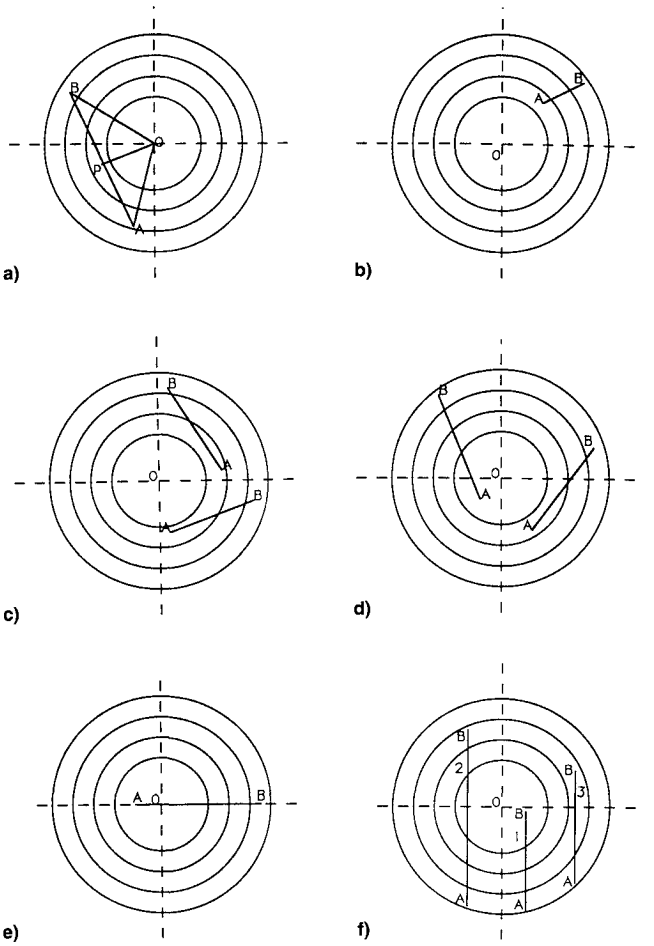

Fig. 3 Possible configurations for calculating the attenuation of the beam in nonhomogeneous medium.

Case vi

Here (Fig. 3f), the slope of $\overline{AB}$ is infinite. Then, the points of intersection are written as

$$x_{1,2} = x_0 \tag{19}$$

$$y_{1,2} = \sqrt{a^2 - x_0^2} \tag{20}$$

Inverse Radiation Problem

In the previous section, the forward (direct) problem is modeled to determine the angular radiosity distribution around the cylindrical particle cloud. The solution to the forward problem is obtained only if the distributions of absorption and scattering coefficients in the medium and the scattering phase function are known. The inverse problem, on the other hand, is to determine these property distributions using the angular radiosity distribution measured from experiments. Here, we will use an optimization scheme to solve the inverse problem in an axisymmetric system. For this purpose, an IMSL regression routine called DBCLSF is employed.[20] This routine uses a modified Levenberg-Marquardt algorithm and a finite difference Jacobian to solve the nonlinear least squares problem. This routine is also used for the inverse Monte-Carlo calculations.[13,19]

The direct problem is solved using known property distributions of the medium and the angular radiosity profile $R_{true}(\theta)$ is determined. These calculations are performed using large number of sublayers (up to 100) in order to simulate the continuous nature of the medium. The calculated radiosities are assumed to be the measurements from experiments and employed as input in the inverse analysis. In order to evaluate the effect of experimental error on the accuracy of the re-

covered properties, the procedure is repeated after introducing a random error to the angular radiosity data $R_{true}(\theta)$.

To start the inverse problem algorithm, first the parameters to be determined are guessed, and using these values the radiosity distribution $\bar{R}(\theta)$ is calculated. Then a function $F(\theta)$ is defined

$$F(\theta) = [R_{true}(\theta) - \bar{R}(\theta)]/R_{true}(\theta)]^{\rho} \quad (21)$$

where ρ is a value between 0 and 1. Based on extensive calculations performed earlier,[13] an optimum value for $\rho(=\frac{1}{2})$ is used. The values of function F are determined by the regression subroutine DBCLSF, which calls the forward solution algorithm to calculate $\bar{R}(\theta)$ function. The forward problem is solved each time to determine an improved radiosity profile using a new set of input parameters. Here, the input parameters to each new solution are determined by the subroutine DBCLSF. Once the function F is minimized, the β and ω parameters used to calculate the final $\bar{R}(\theta)$ function are considered as recovered values.

Typically, the calculations take about 15 CPU minutes on an IBM-3090 computer. However, since the problem is an isolated one, the computational time is not a major drawback, considering the reward of retrieving the information for the radiative property distributions in the medium.

Results and Discussions

In the present study, the inverse problem is solved for three different physical cases. In the first case, the medium is assumed isotropically scattering and the albedo and extinction coefficient distributions are determined. In the second case, a Rayleigh phase function is considered. In the third, a simple linearly anisotropic scattering phase function is employed; the profiles of the albedo and the extinction coefficient, as well as the asymmetry factor of the phase function are recovered.

Table 1 Isotropic scattering (case A)

Parameter	Radius	Input	Recovered
ω_1	$0.0 < r \leq 0.333$	0.8	0.800000
ω_2	$0.333 < r \leq 0.667$	0.5	0.500000
ω_3	$0.667 < r \leq 1.0$	0.2	0.200000
β	$0.0 \leq r \leq 1.0$	0.8	0.800000

Table 2 Isotropic scattering (case A)

Parameter	Radius	Input	Recovered
ω_1	$0.0 < r \leq 0.25$	0.9	0.900000
ω_2	$0.25 < r \leq 0.50$	0.7	0.700000
ω_3	$0.50 < r \leq 0.75$	0.5	0.500000
ω_4	$0.75 < r \leq 1.0$	0.3	0.300000
β	$0.0 \leq r \leq 1.0$	0.8	0.800000

Note that for all the cases considered, the results were not sensitive to the starting values; in the calculations, arbitrary initial values for β and ω parameters were used.

Isotropic Scattering

Case A

Here, a uniform β profile and a step-wise varying ω profile are considered. The cross section of the cylinder is divided into three, four, or five different layers. In each layer, ω is taken as a constant. First, the forward problem is solved. Then, the profiles of the single-scattering albedo and the extinction coefficient are recovered from the inverse analysis. Results for three and four layer systems are shown in Tables 1 and 2. The input and recovered values are identical to six significant digits. These results are based on measurements taken at 11 angular locations for 9 different spatial orientation of laser beam.

To see the effect of a number of observations on the accuracy of the recovered parameters, several more calculations were performed. The results shown in Tables 3 and 4 are given in $M \times N$ format, where M corresponds to number of spatial orientation of the laser beam, and N corresponds to number of angular locations. As expected, with decreasing number of observations, the accuracy decreases; although, even the 5×1 measurements would yield acceptable results. Note, however, for anisotropically scattering, nonhomogeneous system, it is preferable to consider more observations. The results presented below are for $M \times N = 9 \times 11$ measurements.

Case B

In this case, a uniform β and a continuous ω profile in the form of $ar^2 + b$ are considered. In the inverse analysis, the coefficients a and b and the extinction coefficient are recovered. In Table 5, the results for one set of input parameters are listed. The input and recovered values agreed to six significant digits.

Case C

In this case, we considered continuous variations of both ω and β. The cylindrical cross section is divided into 100 layers and in each layer β is assumed uniform. The albedo is considered to vary parabolically. For the inverse analysis, if the cylinder is divided to more than five layers, the optimization routine DBCLSF cannot be used. The reason for this is that the maximum number of parameters which can be recovered effectively, is limited to 10 for the problem being considered. (If more than 10 parameters are optimized, β and ω parameters in some layers either remain unaffected at their initial values or converge to upper or lower bounds, and do not reach the optimum results.) On the other hand, the five-layer system did not show any significant improvement over a four-

Table 3 Isotropic scattering (case A)

			Recovered, $M \times N$		
Parameter	Radius	Input	9×11	5×11	3×11
ω_1	$0.0 < r < 0.333$	0.800	0.800	0.801	0.804
ω_2	$0.333 < r < 0.667$	0.500	0.500	0.499	0.496
ω_3	$0.667 < r < 1.0$	0.200	0.200	0.199	0.369
β	$0.0 < r < 1.0$	0.800	0.800	0.801	0.806

Table 4 Isotropic scattering (case A)

			Recovered, $M \times N$					
Parameter	Radius	Input	9×11	9×6	9×4	9×2	9×1	5×1
ω_1	$0.0 < r < 0.333$	0.800	0.800	0.802	0.801	0.813	0.807	0.809
ω_2	$0.333 < r < 0.667$	0.500	0.500	0.499	0.499	0.502	0.502	0.502
ω_3	$0.667 < r < 1.0$	0.200	0.200	0.199	0.199	0.199	0.199	0.199
β	$0.0 < r < 1.0$	0.800	0.800	0.808	0.810	0.861	0.805	0.808

Table 5 Isotropic scattering (case B)

Parameter	Radius	Input	Recovered
a	—	0.25	0.250000
b	—	0.55	0.550000
β	$0.0 \leq r \leq 1.0$	0.8	0.800000

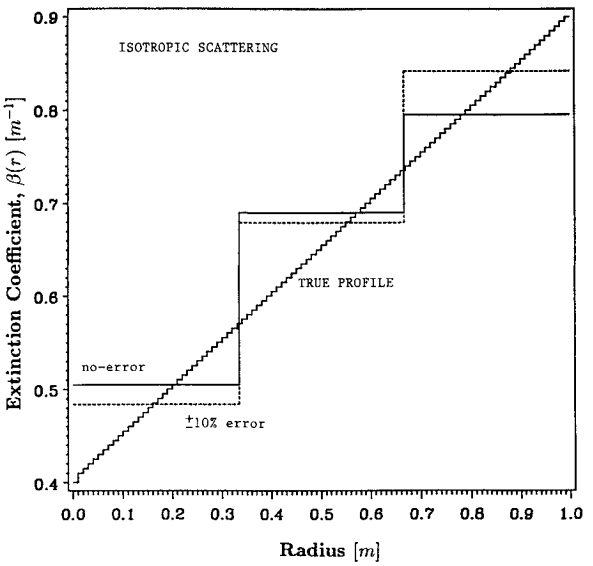

a) Extinction coefficient profiles

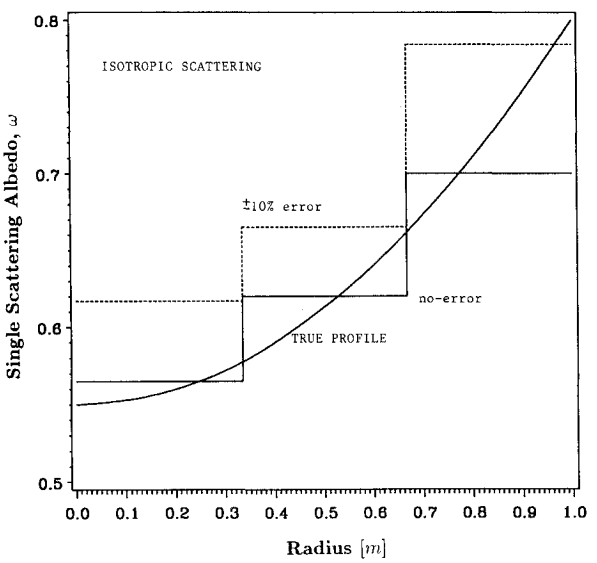

b) Single-scattering albedo profiles

Fig. 4 True and recovered profiles in a three-layer medium (case C). Solid line: no-error in the angular radiosity data used in the inversion; dashed line: random ±10% error in the angular radiosity data.

layer system. Because of this, only the three- and four-layer systems are considered for the inversion.

Figure 4a and 4b depict the input and recovered ω and β profiles for a three-layer system, whereas, Figs. 5a and 5b are for the four-layer system. The results denoted as "no-error" in these figures were obtained assuming no random error in the recorded angular radiosity distribution. In general, the agreement is good, although the accuracy of the recovered values gets worse towards the outside of the medium.

To see the extent of the experimental error on the inverse radiation analysis, a ±10% random error is imposed on the $R(\theta)$ values determined from the forward solution. The input and recovered ω and β profiles for three- and four-layer systems are also depicted in Figs. 4 and 5 with dashed lines (denoted as "±10% error"). The numerical error decreases

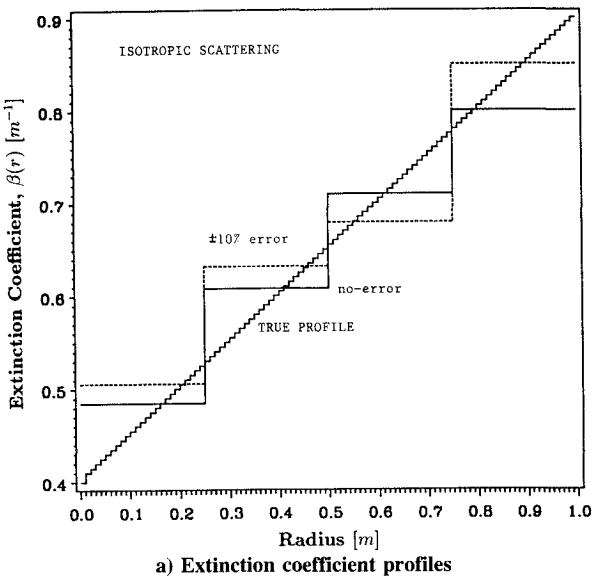

a) Extinction coefficient profiles

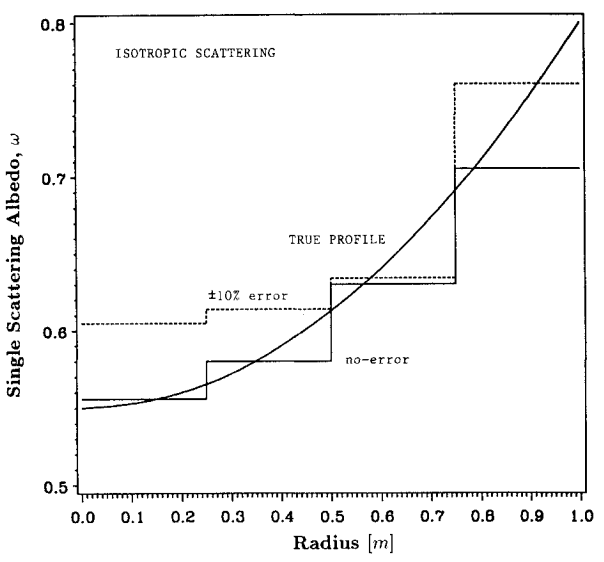

b) Single-scattering albedo profiles

Fig. 5 True and recovered profiles in a four-layer medium (case C). Solid line: no-error in the angular radiosity data used in the inversion; dashed line: random ±10% error in the angular radiosity data.

when the number of uniform layers is increased from three to four.

Rayleigh Scattering

In hydrocarbon flames, soot is the only particle type present in the flame. The size of the individual soot particles is usually very small (less than 100 nm), and assuming individual soot particles are spherical in shape and unagglomerated (which is not always the case), their scattering characteristics can be described with the Rayleigh phase function, which is written as

$$\Phi(\theta) = \tfrac{3}{4}(1 + \cos^2\theta) \tag{22}$$

This phase function is accurate if the size parameter $x = \pi D_{\text{particle}}/\lambda$ is much smaller than 1. In this section, we will investigate the effect of the Rayleigh phase function on the accuracy of the inversion. Note that, in hydrocarbon flames, the radial changes in soot agglomerate size are not very well known; therefore, we will assume that the phase function remains the same across the flame.

Case D

First, a medium with a uniform β and parabolic ω distribution is considered. The forward problem is solved assuming

the particles scatter radiation according to Rayleigh phase function, and in the inverse analysis, β as well as a and b coefficients of the $\omega = ar^2 + b$ profile are recovered. Results, for both no-error and $\pm 10\%$ error cases are listed in Table 6. The error in the recovered a parameter is about 20%, whereas, it is less than 3% for b, if the input data are perturbed. This means that the recovered ω values will have more error towards the edges. For the β value, the error is less than 4%. In general, the agreement between the recovered and the true input data is quite satisfactory.

Case E

In this case, continuous variations of both ω and β are considered (similar to case C). For the solution of the forward problem, the cylindrical cross section is divided into 100 layers, and in each layer β is assumed uniform. The albedo is considered to vary parabolically. In the inverse analysis, a three-layer division is considered for the β profile. The recovered β and $\omega = ar^2 + b$ profiles, with and without random errors, are depicted in Fig. 6 for β, and in Figs. 7a and 7b for ω. Overall, the β profiles are recovered very accurately, even if there is a $\pm 10\%$ error in the input angular radiosity distribution. The same, however, cannot be said for the ω profiles. The main reason for the poor ω results is the crude division of the medium to three-layer system (four layers did not yield any improvement). Because of the limitation of the optimization routine DBCLSF, it was not possible to consider more layers with unknown properties.

Following this, a new approach called successive inversion was applied. The β profile recovered from the analysis (see Fig. 6) is fit to a polynomial and it is assumed to remain invariant. Then, the a and b coefficients of ω profile are recovered. In the inverse analysis, the medium is divided to either 10 or 100 layers. Note that since now β is known, it is possible to divide the medium to many layers; the only unknowns are a and b. The results obtained using the successive inversion scheme are also depicted in Figs. 7. The error in the recovered profile decreases significantly with more layers. Surprisingly, the recovered ω profile with random error in the input data agreed better with the true profile than the no-error case. This better agreement is mainly the result of the optimization used for this particular problem, and should not be considered as a rule. This observation suggests that if there is about $\pm 10\%$ error in the experimental data, the required parameters can still be recovered with a reasonable accuracy.

The successive inversion scheme can be expanded such that both the β and ω profiles are expressed in polynominal form. From the inverse analysis, the coefficients of these polynomials are recovered. This modification requires an explicit relation between the radius-dependent properties [$\beta(r)$ and $\omega(r)$] and path-dependent properties [$\beta(s)$ and $\omega(s)$]. Although such an expression is readily available,[18] because of the extensive computational requirements, this modification was not implemented in the present algorithm.

Table 6 Rayleigh scattering (case D)

Parameter	Radius	Input	Recovered	
			No-error	$\pm 10\%$ Error
a	——	0.25	0.248	0.205
b	——	0.55	0.549	0.564
β	$0.0 \le r \le 1.0$	0.8	0.800	0.829

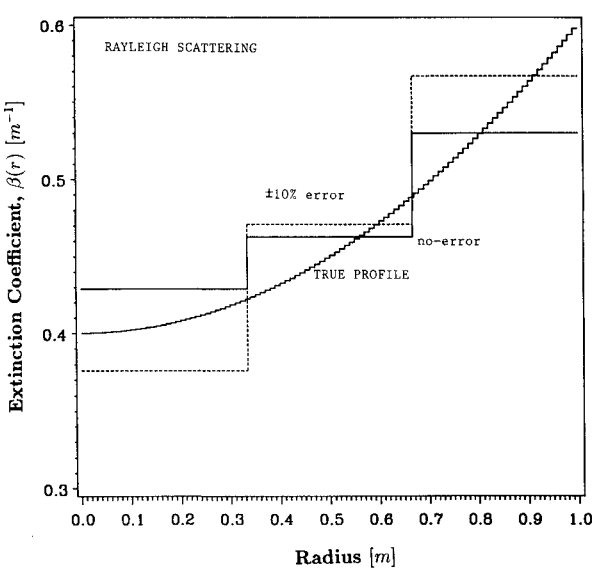

Fig. 6 True and recovered extinction coefficient profiles in a continuous medium (case E). Solid line: no-error in the angular radiosity data used in the inversion; dashed line: random $\pm 10\%$ error in the angular radiosity data.

Linearly Anisotropic Scattering

To study the effect of phase function on the accuracy of the inversion scheme, a simple linearly anisotropic phase function of the form $1 + g\cos(\theta)$ is considered. The asymmetry parameter g is recovered from the inverse analysis, in addition to β and ω. In the present study, only the g values of $+1$ and

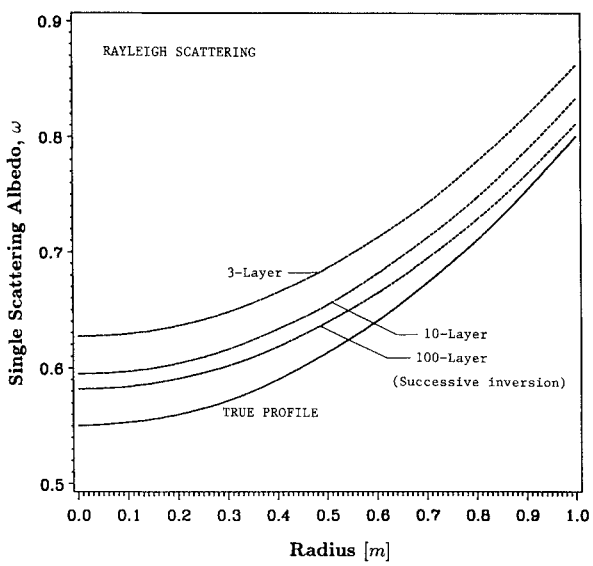

a) No error

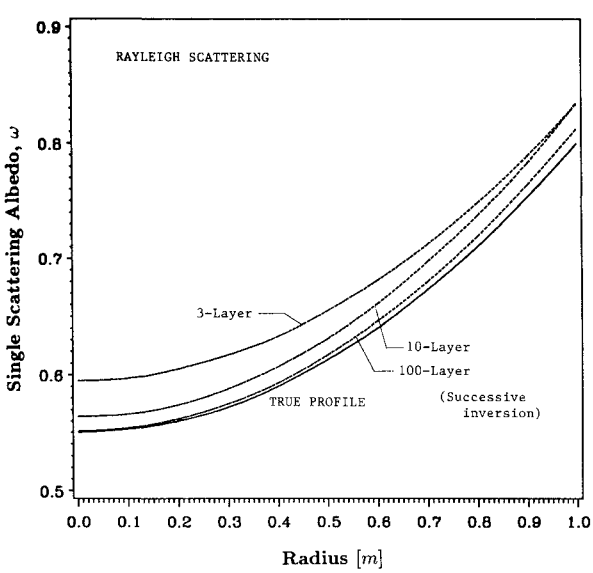

b) −10% Error in input radiosity data

Fig. 7 True and recovered single-scattering albedo profiles; 10 and 100 layer results were obtained with successive inversion (case E).

Table 7 Anisotropic backward scattering (case F)

Parameter	Radius	Input	Recovered	
			No-error	±10% Error
ω_1	$0.0 < r \leq 0.333$	0.55	0.563	0.561
ω_2	$0.333 < r \leq 0.667$	0.65	0.677	0.676
ω_3	$0.667 < r \leq 1.0$	0.75	0.778	0.773
β	$0.0 \leq r \leq 1.0$	0.8	0.804	0.795
g	——	−1.0	−1.002	−1.001

Table 8 Anisotropic forward scattering (case F)

Parameter	Radius	Input	Recovered	
			No-error	±10% Error
ω_1	$0.0 < r \leq 0.333$	0.55	0.563	0.566
ω_2	$0.333 < r \leq 0.667$	0.65	0.675	0.677
ω_3	$0.667 < r \leq 1.0$	0.75	0.776	0.774
β	$0.0 \leq r \leq 1.0$	0.8	0.809	0.819
g	——	1.0	1.001	1.002

Table 9 Anisotropic backward scattering (case G)

Parameter	Radius	Input	Recovered	
			No-error	±10% Error
a	——	0.25	0.275	0.267
b	——	0.55	0.564	0.564
β	$0.0 \leq r \leq 1.0$	0.8	0.801	0.794
g	——	−1.0	−1.001	−1.002

Table 10 Anisotropic forward scattering (case G)

Parameter	Radius	Input	Recovered	
			No-error	±10% Error
a	——	0.25	0.273	0.266
b	——	0.55	0.564	0.566
β	$0.0 \leq r \leq 1.0$	0.8	0.807	0.815
g	——	1.0	1.001	1.002

-1 are considered, which correspond to highly forward and backward scattering particles, respectively.

Case F

The results obtained for a three-layer system are depicted in Tables 7 and 8. This case is similar to case A with one additional parameter, i.e., g. Both no-error and ±10% random error cases are considered. The inverse analysis works very well for these two cases. Even with error in the input radiosities, the recovered values are accurate within a few percent of the input.

Case G

In this case, the extinction coefficient is assumed uniform, and the albedo is varied parabolically, in the form of $ar^2 + b$. Tables 9 and 10 list the input and recovered values of a, b, β, and g. For both cases considered ($g = +1$ and -1) the error never exceeds 7% in any of the recovered parameters.

Conclusions

A simple semianalytical scheme for the solution of the inverse radiation problem to recover the extinction coefficient and single-scattering albedo profiles in an axisymmetric, cylindrical medium is presented. Isotropic scattering, Rayleigh scattering, and linearly anisotropic scattering phase functions are considered in the analysis. The results indicate that the worst error in recovered properties is usually less than 10%, even if there is a random 10% error in input radiosities.

The main limitation of the methodology is that only a small number of unknown parameters can be recovered using the IMSL routine DBCLSF. This means that we need to consider a crude step-profile for both β and ω in the inverse analysis. However, this approach yields poor results for the albedo profile. This limitation can be overcome to a great extent by employing the "successive inversion" scheme.

Acknowledgments

This work was partially supported by the Department of Energy Grant DE-FG22-87PC79916 and the National Science Foundation Grant CBT-870867.

References

[1]Chen, F. P., and Goulard, R., "Retrieval of Arbitrary Concentration and Temperature Fields by Multiangular Scanning Techniques," *Journal of Quantitative Spectroscopy and Radiative Transfer*, Vol. 16, 1976, pp. 819–827.

[2]Hughey, B. J., and Santavicca, D. A., "A Comparison of Techniques for Reconstructing Axisymmetric Flow Fields from Absorption Measurements," *Combustion Science and Technology*, Vol. 29, Houston, TX, 1982, p. 167.

[3]Chakravarty, S., Mengüç, M. P., Mackowski, D. W., and Altenkirch, R. A., "Application of Two Inversion Schemes to Determine the Absorption Coefficient Distribution in Flames," *Proceedings of the ASME National Heat Transfer Conference*, edited by H. R. Jacobs, Vol. 1, 1988, pp. 171–178.

[4]Barett, H. H., and Swindel, W., "Analog Reconstruction Methods for Transaxial Tomography," *Proceedings IEEE*, Vol. 65, 1977, p. 89.

[5]Emmermann, P. J., Goulard, R., Santoro, R. J., and Semerjian, H. G., "Multiangular Absorption Diagnostics of a Turbulent Argon-Methane Jet," *AIAA Proceedings*, March–April, 1980, pp. 70–77.

[6]Santoro, R. J., Semerjian, H. G., Emmermann, P. J., and Goulard, R., "Optical Tomography for Flow Field Diagnostics," *International Journal of Heat and Mass Transfer*, Vol. 24, 1981, pp. 1139–1150.

[7]Santoro, R. J., Semerjian, H. G., and Dobbins, R. A., "Soot Particle Measurement in Diffusion Flames," *Combustion and Flame*, Vol. 51, 1983, pp. 203–218.

[8]Ravichandran, M. R., and Gouldin, F. C., "Determination of Temperature and Concentration Profiles Using (a Limited Number of) Absorption Measurements," *Combustion Science and Technology*, Vol. 45, 1986, p. 47.

[9]Mengüç, M. P., and Dutta, P., "Scattering Tomography and Application of Sooting Diffusion Flames," ASME/AIChE National Heat Transfer Conf., San Diego, CA, Aug. 1992.

[10]McCormick, N. J., "A Critique of Inverse Solutions to Slab Geometry Transport Problems," *Progress in Nuclear Energy*, Vol. 8, 1981, pp. 235–245.

[11]McCormick, N. J., "Recent Developments in Inverse Scattering Transport Methods," *Transport Theory and Statistical Physics*, Vol. 13, 1984, pp. 15–28.

[12]McCormick, N. J., "Methods for Solving Inverse Problems for Radiation Transport—An Update," *Transport Theory and Statistical Physics*, Vol. 15, 1986, pp. 759–772.

[13]Subramaniam, S., and Mengüç, M. P., "Solution of Inverse Radiation Problem for Inhomogeneous and Anisotropically Scattering Media Using a Monte Carlo Technique," *International Journal of Heat and Mass Transfer*, Vol. 34, 1991, pp. 253–266.

[14]Dunn, W. L., "Inverse Monte Carlo Solutions for Radiative Transfer in Inhomogeneous Media," *Journal of Quantitative Spectroscopy and Radiative Transfer*, Vol. 29, 1983, pp. 19–26.

[15]Ho, C.-H., and Özişik, M. N., "Inverse Radiation Problems in Inhomogeneous Media," *Journal of Quantitative Spectroscopy and Radiative Transfer*, Vol. 40, 1988, pp. 553–560.

[16]Larsen, E. W., "Solution of Multidimensional Inverse Transport Problems," *Journal of Mathematical Physics*, Vol. 25, 1984, pp. 131–135.

[17]Larsen, E. W., "Solution of Three-Dimensional Inverse Transport Problems," *Transport Theory and Statistical Physics*, Vol. 17, 1988, pp. 147–167.

[18]Mengüç, M. P., "Scattering Tomography: A Tomographic Reconstruction Technique for Radially Inhomogeneous Scattering Media," 1993.

[19]Mengüç, M. P., and Sitaraman, S., "Monte-Carlo Solution to Inverse Radiation Problem in Radially Inhomogeneous Anisotropically Scattering Media," 1993.

[20]*IMSL Library*, 10th ed., NBC Building, Houston, TX, 1987.

[21]Agarwal, B., and Mengüç, M. P., "Forward and Inverse Analysis of Single and Multiple Scattering of Collimated Radiation in an Axisymmetric System," *International Journal of Heat and Mass Transfer*, Vol. 34, 1991, pp. 633–647.